The Astrophysical Journal Letters, 804:L42 (7pp), 2015 May 10 doi:10.1088/2041-8205/804/2/L42

FROM OUTSIDE-IN TO INSIDE-OUT: GALAXY ASSEMBLY MODE DEPENDS ON STELLAR MASS

Zhizheng Pan[1], Jinrong Li[2,3], Weipeng Lin[1,5], Jing Wang[4], Lulu Fan[2,3], and Xu Kong[2,3]
[1] Key Laboratory for Research in Galaxies and Cosmology, Shanghai Astronomical Observatory, Chinese Academy of Sciences, 80 Nandan Road, Shanghai 200030, China; panzz@shao.ac.cn, linwp@shao.ac.cn
[2] Center of Astrophysics, University of Science and Technology of China, Jinzhai Road 96, Hefei 230026, China; xkong@ustc.edu.cn
[3] Key Laboratory for Research in Galaxies and Cosmology, USTC, CAS, China
[4] CSIRO Astronomy & Space Science, Australia Telescope National Facility, P.O. Box 76, Epping, NSW 1710, Australia
[5] School of Astronomy and Space Science, Sun Yat-Sen University, Guangzhou 510275, China
Received 2015 March 30; accepted 2015 April 24; published 2015 May 11

ABSTRACT

In this Letter, we investigate how galaxy mass assembly mode depends on stellar mass M_* using a large sample of ~10,000 low-redshift galaxies. Our galaxy sample is selected to have SDSS $R_{90} > 5.''0$, which allows the measures of both the integrated and the central NUV–r color indices. We find that in the M_*–(NUV–r) green valley (GV), the $M_* < 10^{10}\,M_\odot$ galaxies mostly have positive or flat color gradients, while most of the $M_* > 10^{10.5}\,M_\odot$ galaxies have negative color gradients. When their central D_n4000 index values exceed 1.6, the $M_* < 10^{10.0}\,M_\odot$ galaxies have moved to the UV red sequence, whereas a large fraction of the $M_* > 10^{10.5}\,M_\odot$ galaxies still lie on the UV blue cloud or the GV region. We conclude that the main galaxy assembly mode is transiting from "the outside-in" mode to "the inside-out" mode at $M_* < 10^{10}\,M_\odot$ and at $M_* > 10^{10.5}\,M_\odot$. We argue that the physical origin of this is the compromise between the internal and the external processes that drive the star formation quenching in galaxies. These results can be checked with the upcoming large data produced by the ongoing integral field spectroscopic survey projects, such as CALIFA, MaNGA, and SAMI in the near future.

Key words: galaxies: evolution – galaxies: star formation

1. INTRODUCTION

The stellar mass of a galaxy, M_*, is one of its most fundamental properties. The assembly of M_* is a long-standing issue in the field of galaxy formation and evolution. To elucidate how M_* evolves, one would expect to recover the star formation history (SFH), both in space and time, for individual galaxies. In practice, the SFH of a galaxy is determined by finding the most plausible combination of evolved single stellar populations that matches its observed spectrum or spectral energy distribution. This so-called "fossil record method" has been widely applied to the integral field spectroscopic (IFS) data and the multi-band images with good spatial coverage to study galaxy assembly (Kong et al. 2000; Cid Fernandes et al. 2013; Lin et al. 2013; Pérez et al. 2013).

Previous works have found two distinct stellar mass assembly modes. They are termed as "the inside-out" and "the outside-in" modes in the literature (Sánchez-Blázquez et al. 2007; Pérez et al. 2013). In the "inside-out" scenario, mass assembly is first finished in the galactic central region. For instance, in a young disk galaxy, the disk instability will induce gas inflow and trigger starburst in the galactic center as it evolves. Besides star formation, the inflow gas can also fuel the central supermassive black hole. The subsequent active galactic nucleus (AGN) feedback (such as blowing the gas out of the galaxy or heating it against cooling down to form new stars) will then suppress the central star formation, leaving a compact, quiescent galactic bulge (Bournaud et al. 2014; Dekel & Burkert 2014). Compared to the central part, its outskirts form through a much gentler process, such as the star formation driven by the gradual accretion of cold inter galactic medium, or the accretion of small satellite galaxies. Many works found that massive spiral galaxies have negative color or stellar age gradients, supporting this picture (Wang et al. 2011; Lin et al. 2013; Pérez et al. 2013; Sánchez-Blázquez et al. 2014). Compared to their massive counterparts, low-mass galaxies have much shallower potential wells, making them less capable of retrieving the gas blowing by the galactic outflows or accreting cold gas to form new stars. In addition, the role of AGN feedback may not be so efficient in low-mass galaxies, as their AGN occupation fraction is very low (Kauffmann et al. 2003b). Thus, it is not surprising to see that the low-mass galaxies have a different mass assembly mode. In fact, observations show that the evolution of low-mass galaxies can be better interpreted in an "outside-in" framework (Gallart et al. 2008; Zhang et al. 2012).

It is now clear that the galaxy assembly mode has dependence on its already formed M_*. Nevertheless, we know less about whether or not there is a mass threshold that can roughly separate these two distinct modes. Answering this question requires the investigation of a sufficiently large sample, which expands a wide mass range. Recently, using the IFS data of 105 galaxies observed by the CALIFA project (Sánchez et al. 2012), Pérez et al. (2013) found that galaxies more massive than $5 \times 10^{9.0}\,M_\odot$ grow inside-out, while lower-mass galaxies grow outside-in. However, this sample is still relatively modest, and there are only about 20 galaxies with $M_* < 10^{10}\,M_\odot$ galaxies in this sample (see their Figure 1). To study a larger sample, in this Letter, we use the *GALEX* (Martin et al. 2005) photometry, combined with the SDSS (York et al. 2000) data, to investigate how galaxy assembly mode depends on stellar mass. Throughout this Letter, we assume a concordance ΛCDM cosmology with $\Omega_m = 0.3$, $\Omega_\Lambda = 0.7$, $H_0 = 70\,\mathrm{km\,s^{-1}\,Mpc^{-1}}$, and a Kroupa (2001) IMF.

2. METHOD AND DATA USED

In this Letter, we will investigate the stellar age in the central region, as well that of the global, in individual galaxies. For a

galaxy, by comparing these two quantities, we can investigate whether its central part is first assembled. Traditionally, stellar age is determined using broad-band optical photometry when spectral information is not available. However, the use of optical photometry has been plagued by the well-known age–metallicity degeneracy (AMD) whereby young, metal-rich stellar populations produce optical colors that are indistinguishable from those produced by old, metal-poor populations (Worthey 1994). To avoid the AMD, we use the NUV–r color index as a stellar age indicator since it is sensitive to low-level recent star formation (RSF), but is unaffected by the AMD when stellar age is <1 Gyr (Kaviraj et al. 2007a, 2007b).

Following the Wang et al. (2010) pipeline, we have constructed a UV–optical matched photometric catalog. This catalog contains about 220,000 galaxies with uniform photometric measurements on the resolution and point-spread function (PSF)-matched *GALEX*+SDSS images, which are cross-matched by the SDSS DR8 (Aihara et al. 2011) spectroscopic galaxies and the *GALEX* GR6 database. For each galaxy, the fluxes were measured over five different apertures, with $r = [1.5, 3.0, 6.0, 9.0, 12.0]$ ″, in the FUV, NUV, u, g, r, i, z bands. Along with the aperture photometry, we also measure the total magnitudes of the galaxies with SExtractor (Bertin & Arnouts 1996). All the magnitudes have been corrected for galactic extinction using the galactic dust map (Schlegel et al. 1998). The data reduction procedure is refereed to Wang et al. (2010) and Pan et al. (2014).

To measure the NUV–r color index in the central region of a galaxy, one would expect the galaxy to be spatially resolved in both the *GALEX* and SDSS images. The *GALEX* NUV image has a pixel size of 1 pixel = 1.″5 and a PSF with FWHM = 5.″3. The pixel size and PSF of the SDSS image are 0.″396 and 1.″4, respectively. To ensure that the measured central NUV–r color index is not significantly affected by the relatively poor resolution of the *GALEX* images, the chosen central aperture should not be smaller than the NUV PSF, e.g., $r_{\rm central}$ should not be smaller than 5.″3/2 ≈ 2.″7. In the five apertures, the $r = 3.''0$ aperture is thus most suitable to be chosen as the "central aperture." Then, we select the galaxies passing the following as our parent sample: (1) SDSS minor–major axis ration $b/a > 0.5$; (2) SDSS $R_{90} > 5.''0$, where R_{90} is the radii-enclosed 90% of the SDSS r-band Petrosian flux; (3) $z = [0.005, 0.05]$, where z is SDSS spectroscopic redshift; and (4) $m_{\rm NUV} < m_{\rm limit}$, where $m_{\rm limit} = 23.0$ mag is the limited magnitude in the NUV band. The limit on b/a is to minimize the dust reddening effect on our results. Finally, we limit these galaxies to have stellar mass $M_* > 10^{9.0}\,M_\odot$ to form a volume-completed sample at $z < 0.05$ (Schawinski et al. 2010). The final sample size is $N_{\rm gal} = 11{,}294$. The stellar mass M_* and the spectral index D_n4000 used in this Letter were drawn from the JHU/MPA database.[6]

In the upper pannel of Figure 1, we show the central flux fraction ($f_{\rm central}$) distribution for our sample, where $f_{\rm central}$ was defined as $f_{\rm central} = {\rm Flux}_{r=3.''0}/{\rm Flux}_{\rm total}$. It can be seen that in the SDSS r band, the median value of $f_{\rm central}$ is ∼0.25. One will also find that the $f_{\rm central}$ distribution is much broader in the NUV band. The Kolmogorov–Smirnoff test on these two distributions gives a small probability (<0.01) that they are drawn from the same distribution. This may be due to the highly different RSF in the galaxy central regions. Figure 1 illustrates that even for the $R_{90} \approx 5.''0$ galaxies, in the SDSS r band, their $f_{\rm central}$ are not higher than 0.4. Thus, for this galaxy sample, our chosen central aperture should be appropriate.

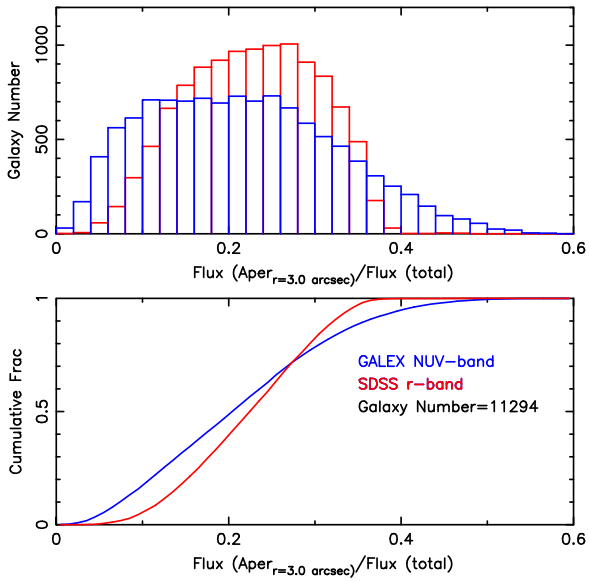

Figure 1. Upper panel: the $f_{\rm central}$ distribution for our sample, where $f_{\rm central}$ was defined as $f_{\rm central} = {\rm Flux}_{r=3.''0}/{\rm Flux}_{\rm total}$. The *GALEX* NUV and SDSS r band is shown as blue and red histograms, respectively. Lower panel: the cumulative curve of $f_{\rm central}$.

3. RESULTS

3.1. The Color–Magnitude Diagram

The color–magnitude diagram, or the color–mass diagram (CMD), used to diagnose the galaxy evolutional stage is widespread in the literature (Faber et al. 2007; Kaviraj et al. 2007b; Schawinski et al. 2014). Based on their positions on the CMD, galaxies can be roughly categorized into two main populations, e.g., the red-sequence galaxies and blue-cloud galaxies. Galaxies that lie between the "blue cloud" and "red sequence," are called the "green valley" (GV) galaxies (Strateva et al. 2001; Baldry et al. 2004). GV galaxies were traditionally thought to be the transition populations between the star-forming and the quenched galaxies (Mok et al. 2013; Pan et al. 2013, 2014; Schawinski et al. 2014; Vulcani et al. 2015). To show the CMD clearly, we have divided the sample into three subsamples, according to their Δ NUV–r, where $\Delta{\rm NUV}-r = ({\rm NUV}-r_{r=3.''0})-({\rm NUV}-r_{\rm total})$. ${\rm NUV}-r_{r=3.''0}$ and ${\rm NUV}-r_{\rm total}$ are the color indices measured in the central $r = 3.''0$ aperture and that of the whole galaxy, respectively. The typical error of Δ NUV–r, σ_0, is derived as $\int_0^{\sigma_0} N(\sigma)/N_{\rm gal}\,d\sigma = 0.80$, where $N(\sigma)$ is the number of galaxies with a Δ NUV–r error of σ. For this sample, σ_0 is 0.15 mag. In what follows, we called galaxies with $\Delta{\rm NUV}-r > 2\sigma_0$ "red-cored" galaxies. The "blue-cored" galaxies are those with $\Delta{\rm NUV}-r < -2\sigma_0$. They are denoted with red and blue symbols in panel (a) of Figure 2, respectively. Those galaxies with flat color gradients, e.g., galaxies with $|\Delta{\rm NUV}-r| < 2\sigma_0$, are shown with green symbols. All AGNs in our sample are narrow-line (obscured) AGNs, so there should be no contribution from the AGN continuum to the NUV–r color index.

In panels (b)–(d) of Figure 2, we show the M_*– (NUV–r) diagram for the blue-cored, flat-gradient, and red-cored

[6] http://www.mpa-garching.mpg.de/SDSS/DR7

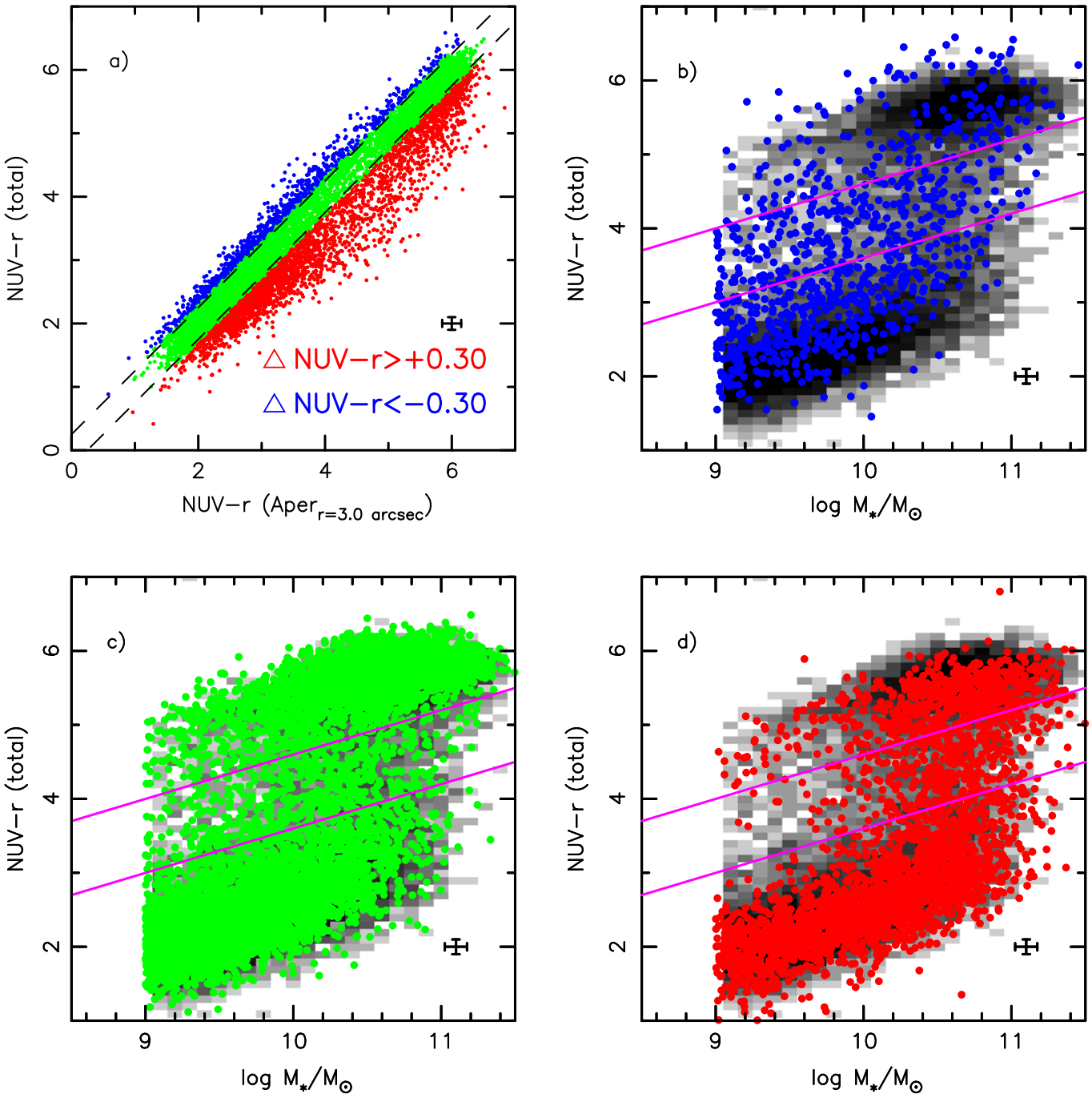

Figure 2. (a) Relation between NUV$-r_{r=3''0}$ and NUV$-r_{\rm total}$, where NUV$-r_{r=3''0}$ and NUV$-r_{\rm total}$ are the color indices measured in the central $r = 3''0$ aperture and that of the whole galaxy, respectively. ΔNUV$-r$ is defined as ΔNUV$-r$ = (NUV$-r_{r=3''0}$)−(NUV$-r_{\rm total}$). (b) The M_* vs. NUV$-r$ (total) diagram for galaxies with ΔNUV$-r < -0.3$. (c) CMD for galaxies with $-0.3 < \Delta$ NUV$-r < 0.3$. (d) CMD for galaxies with Δ NUV$-r > 0.3$. The two pink lines denote our "green valley" definition.

galaxies, respectively. The grayscale represents the galaxy number density of the *whole* sample. On the CMD, one can see the evident "color bimodality." The GV region is arbitrarily defined by the two pink lines, with $0.6 \times M_* - 2.4 < ({\rm NUV} - r)_{\rm GV} < 0.6 \times M_* - 1.4$, where M_* is logarithm stellar mass. As shown in Kaviraj et al. (2007a), galaxies with an NUV–r color less than 5.0 are very likely to have experienced RSF. In the blue cloud and GV region, the "blue-cored" phenomenon thus corresponds to centrally concentrated star formation. In panel (c), we show that flat-gradient galaxies distributed similarly to the whole sample on the CMD. This is expected since they are most numerous. Strikingly, panel (d) shows that there are nearly no "red-cored" galaxies in the GV region below $M_* \sim 10^{10.0}\,M_\odot$.

In Figure 3, we show the fractions of the three kinds of galaxies, scaled with M_*, in the blue cloud, GV, and red sequence. It is clear from Figure 3 that at $M_* > 10^{10.5}\,M_\odot$, the blue cloud and GV region are mostly populated by red-cored galaxies. In the GV region, we see a significant increase of blue-cored $M_* < 10^{10.0}\,M_\odot$ galaxies when compared to the

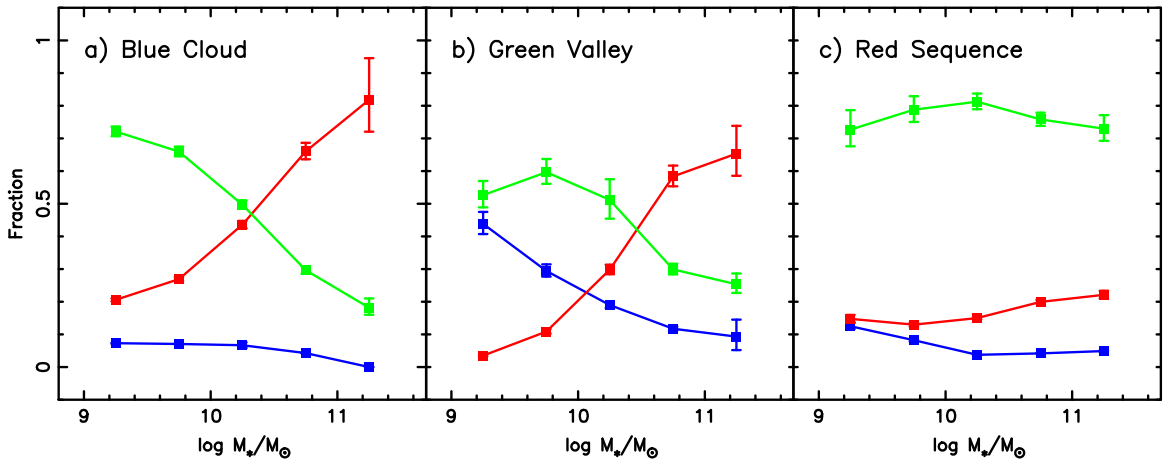

Figure 3. Fractions of blue-cored (blue symbols), flat-gradient (green symbols), and red-cored (red symbols) galaxies as a function of M_*. From left to right, we show the results for the blue cloud, green valley, and red sequence. Errors are derived from 100 bootstrap resamplings.

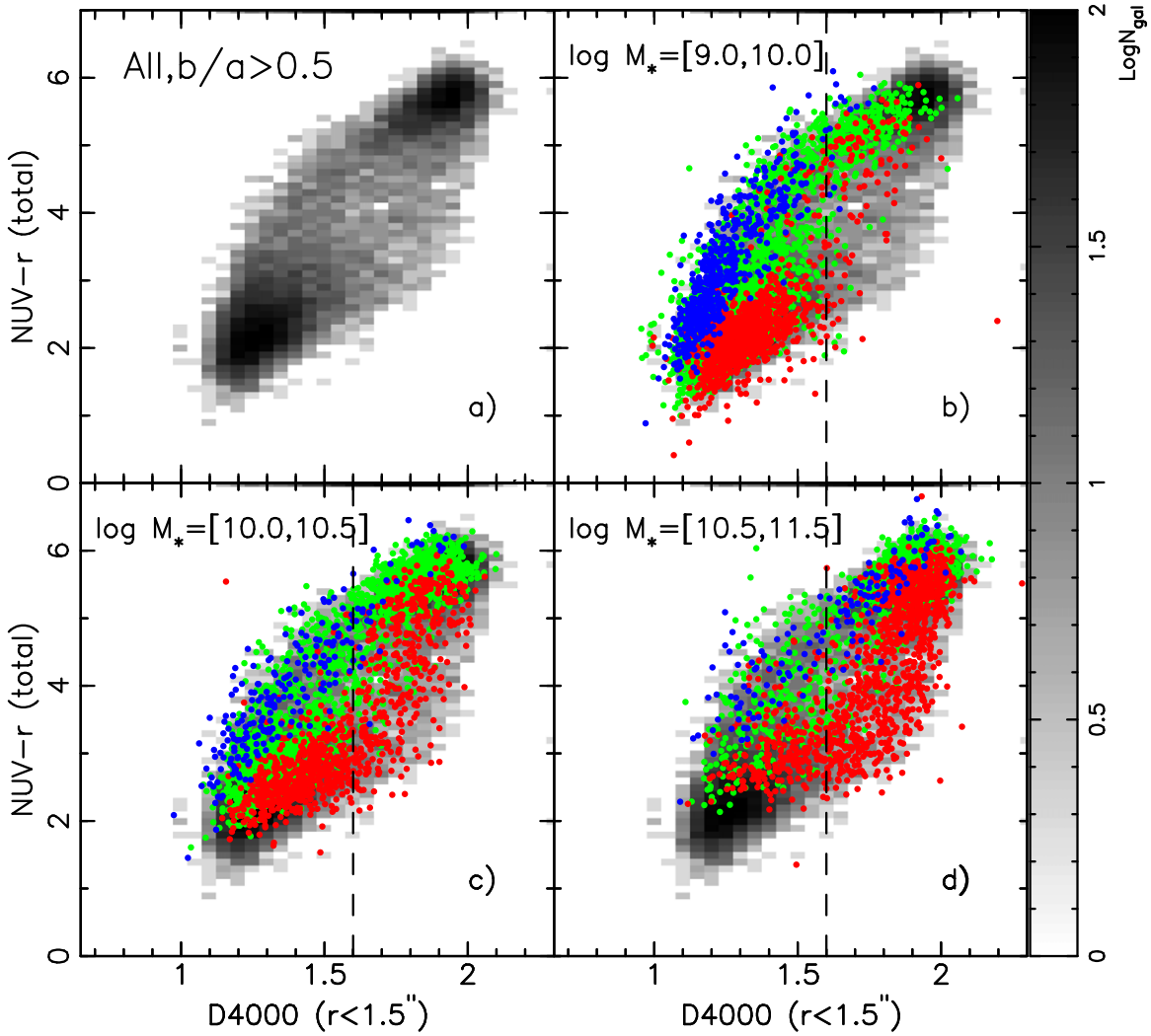

Figure 4. Panel (a): the central D_n4000 vs. NUV–r (total) relation for the whole sample. Panels (b)–(d) show this relation for the log $M_*/M_\odot$ < 10.0, log $M_*/M_\odot$ = [10.0,10.5] and log $M_*/M_\odot$ > 10.5 subsamples, respectively. Color symbols are the same as in Figure 2.

blue cloud, at the expense of a decrease of red-cored and flat-gradient galaxies. This can be interpreted as the outside-in quenching processes (regardless of its working mechanisms) transforming a significant fraction of the red-cored and flat-gradient galaxies into blue-cored ones and driving them to evolve from blue cloud to GV. In the red sequence, galaxies mostly have flat color gradients. This is expected since the NUV–r color index is not sensitive to stellar age that is older

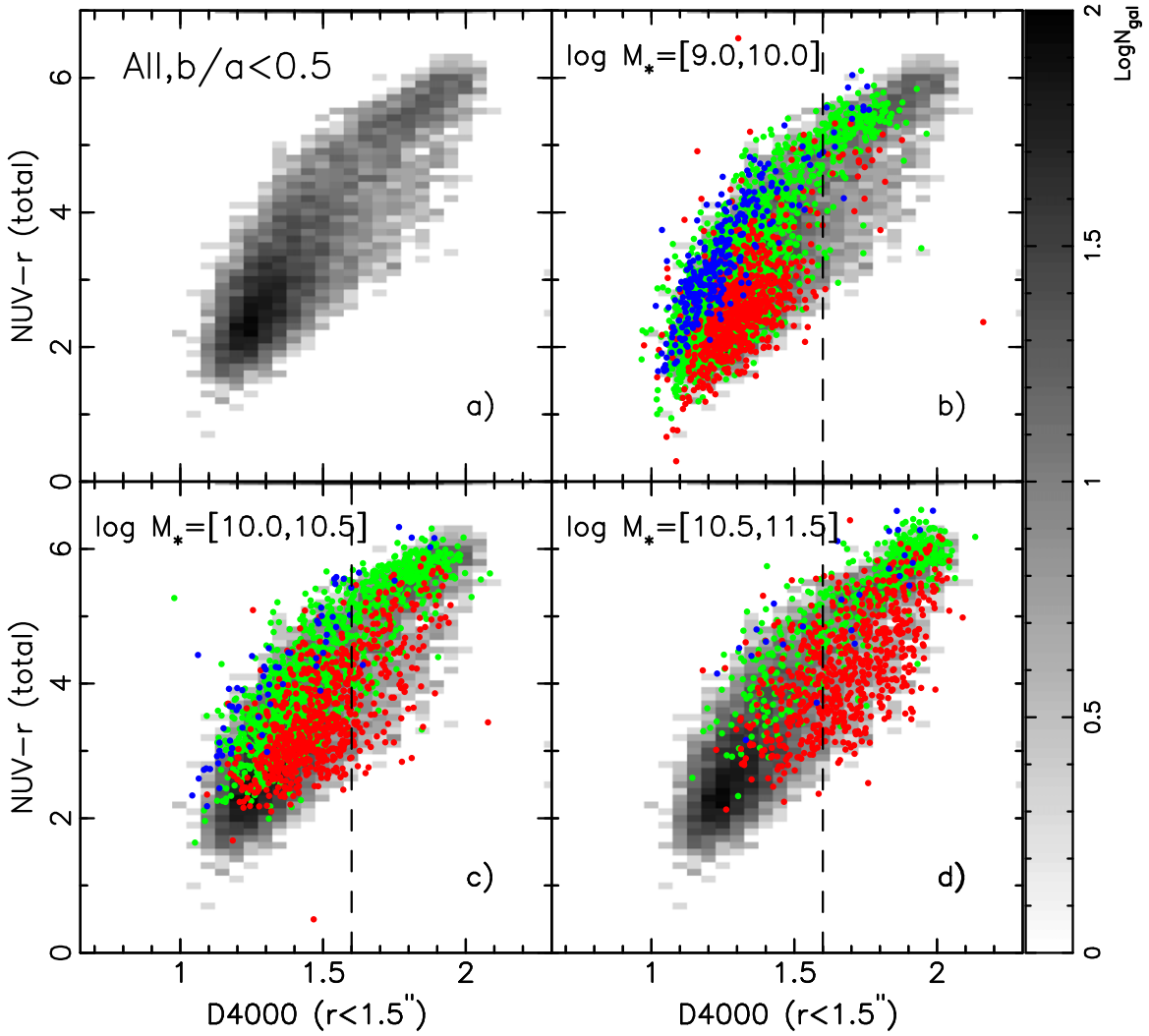

Figure 5. Same as Figure 4, but shown for the inclined galaxies.

than 1 Gyr (Kaviraj et al. 2007b). In summary, Figures 2 and 3 confirm the findings of Pérez et al. (2013) that $M_* < 10^{10.0}\,M_\odot$ galaxies mainly grow "outside-in." The importance of the "inside-out" mode steadily increases with M_* and becomes dominant at around $M_* > 10^{10.5}\,M_\odot$.

3.2. D_n4000 versus NUV–r Diagram

In this section, we will use a spectroscopic index, the D_n4000 index measured from the SDSS $r = 1\farcs5$ aperture spectra, as a central stellar age indicator. The D_n4000 is widely used as a mean stellar age indicator in the literature since it is sensitive to the ratio of present to past average star formation rate (Kauffmann et al. 2003a; Brinchmann et al. 2004), but is less affected by dust and metallicity.

In panel (a) of Figure 4, we show the D_n4000 versus NUV–r (total) relation for our sample. The grayscale represents the number density of galaxies. We can see that there is a positive relation between D_n4000 and NUV–r (total), as is also found in Kauffmann et al. (2007). The scatter of this relation reaches its maximum at NUV–$r \approx$ [3.0, 5.0], e.g., the GV region of the CMD. In panels (b)–(d), we show the D_n4000 versus NUV–r (total) relation for three subsamples, which are binned according to their M_*. The color-coded symbols are the same as those in Figure 2. In Figure 4, one can find that the red and the blue symbols are still separable. This confirms that the NUV$-r_{r=3\farcs0}$ is equivalent to the SDSS D_n4000 index.

In panel (b) of Figure 4, we find that nearly all of the $M_* < 10^{10.0}\,M_\odot$ galaxies have moved to the red sequence when their central $D_n4000 > 1.6$. In contrast, in panel (d), we find that a large portion of the $M_* > 10^{10.5}\,M_\odot$ galaxies still lie on the blue cloud or the GV region when their central $D_n4000 > 1.6$. Panels (b) and (d) together show that there seems to be two separable evolution paths through which the blue-cloud galaxies evolve into the red sequence. In this work, it is natural to interpret these two paths as "outside-in" and "inside-out," respectively.

In panel (b), we show that the flat-gradient galaxies are on the same path as those of "blue-cored" galaxies. Due to the the accurate measurements of D_n4000 and NUV–r (total), we can now conclude that at $M_* < 10^{10.0}\,M_\odot$, the flat-gradient galaxies follow a similar evolutionary path to the "blue-cored" when they move to the red sequence, e.g., they evolve "outside-in."

A potential issue that may affect the result of Figure 4 is that we have not applied dust reddening correction to the NUV–r (total) color index. Since the color index of the inclined galaxies is more easily reddened by the galactic dust lanes, to

assess the role of dust on our result, we show the D_n4000 versus NUV−r (total) relation for the $b/a < 0.5$ galaxies in Figure 5. By comparing Figures 4 and 5, we find that the result is not changed for the $M_* < 10^{10.0}\,M_\odot$ galaxies. At $D_n4000 > 1.6$, many $M_* > 10^{10.5}\,M_\odot$ galaxies are reddened by dust, but their distributions can still be separated from those of the $M_* < 10^{10.0}\,M_\odot$ on this diagram. This test suggests that the two separable paths revealed in Figure 4 are intrinsic.

4. SUMMARY AND DISCUSSION

In this Letter, we investigate how galaxy mass assembly mode depends on stellar mass M_* using a large sample of ∼10,000 low-redshift galaxies. The use of *GALEX* photometry and SDSS data enables us to study a large sample without the IFS data. We compare the stellar age indicator measured in the galactic centers to that of the whole galaxy to determine whether the galaxy grows "outside-in" or "inside-out." We find that in the M_*–(NUV–r) GV, the $M_* < 10^{10}\,M_\odot$ galaxies are mostly "blue-cored" or have flat color gradients, whereas the $M_* > 10^{10.5}\,M_\odot$ galaxies are "red-cored." When their central D_n4000 index values exceed 1.6, the $M_* < 10^{10.0}\,M_\odot$ galaxies have lain on the UV red sequence, whereas a large fraction of the $M_* > 10^{10.5}\,M_\odot$ galaxies still lie on the UV blue cloud or the GV region. These findings suggest that the main galaxy assembly mode is transiting from "the outside-in" mode to "the inside-out" mode at $M_* < 10^{10}\,M_\odot$ and $M_* > 10^{10.5}\,M_\odot$.

We interpret these results as a compromise between the internal and external processes that drive star formation quenching in galaxies. The internal process, like the AGN feedback (e.g., Croton et al. 2006) and the supernova feedback induced from the strong starburst activity (Geach et al. 2014), can blow the gas out of the galactic center, causing the "inside-out" evolution. The external process, like the environmental effects, will strip the gas content of galaxies first from their outskirts, causing the "outside-in" evolution. A galaxy can retrieve the lost gas, or accreting new gas that rebuilds its outskirts, due to its gravity. It is thus not surprising to see that the galaxy assembly modes have a strong dependence on M_*.

Panel (b) of Figure 2 shows that a significant fraction of the $M_* < 10^{10.5}\,M_\odot$ galaxies are "blue-cored." Previous works found that galaxies of this type are usually bulge-dominated systems, like the E+A galaxies (Yang et al. 2008) or the early-type galaxies (Lisker et al. 2007; Suh et al. 2010; Pan et al. 2014). This phenomenon can either be explained as the "survived" star formation of an late-type galaxy that is suffering gas stripping or as the "excess" central star formation, probably triggered in a merge event. Since the merge rate is rare in the local universe, we suggest that the "survived star formation" explanation is the case for the majority of the "blue-cored" galaxies, especially for the low-mass ones.

Since $M_* < 10^{10}\,M_\odot$, galaxies are mostly satellites of massive halos. In a group/cluster environment, ram pressure stripping (Gunn & Gott 1972) and tidal interactions can remove the gas from galaxies, especially for those with low stellar mass densities (Zhang et al. 2013). Other gentler processes, such as "starvation" and "harassment," are also at work (Barazza et al. 2002; Weinmann et al. 2009). The important role of dense environment on the formation of red dwarf galaxies is confirmed by the works focused on the Virgo and Coma clusters (see Boselli & Gavazzi 2014 for a review). At lower halo mass, Geha et al. (2012) found that quenched $M_* < 10^9\,M_\odot$ galaxies do not exist in the field, suggesting that the internal process alone is not sufficient in quenching star formation of low-mass galaxies. At higher redshifts, using the COSMOS data, Pan et al. (2013) found that the important role of environment on the evolution of $M_* < 10^{10}\,M_\odot$ galaxies takes place at $z < 0.7$.

The hierarchical paradigm for galaxy formation implies that galaxies experience a variety of environments during their evolution and may have complex SFH at their early assembly epoch. In Figures 2 and 4, we find that there are many "red-cored" dwarf galaxies in the blue cloud. However, these galaxies are not quenched, even their cores are older than the global. It is worth mentioning why we focus on the GV galaxies at this point. GV galaxies are closer to the "fully assembled" stage than the blue-cloud galaxies (here, we do not include those GV galaxies due to "rejuvenation"), hence holding important clues to the galaxy's final assembly process. As can be seen in panel (a) of Figure 4, when galaxies evolved into the GV region, there seems to be two separable paths connecting the blue cloud and the red sequence. This is expected if there is a dichotomy in the galaxy assembly modes.

We find that the log $M_*/M_\odot = [10.0, 10.5]$ regime is a transition zone. This is not reported in Pérez et al. (2013), probably due to their small sample size. Since the sample used in this Letter is ∼100 times larger than that in Pérez et al. (2013), our results should be reliable in a statistical sense. At higher masses, our finding is in generally consistent with previous studies. The results of our work can be re-examined using the upcoming large data produced by the ongoing IFS survey projects, such as CALIFA, MaNGA, and SAMI, in the near future.

We thank the anonymous referee for the constructive report. This work was supported by the NSFC projects (grant Nos. 11473053, 11121062, 11233005, U1331201, 11225315, 1320101002, 11433005, and 11421303), the National Key Basic Research Program of China (grant No. 2015CB857001), the "Strategic Priority Research Program the Emergence of Cosmological Structures" of the Chinese Academy of Sciences (grant No. XDB09000000), the Specialized Research Fund for the Doctoral Program of Higher Education (SRFDP; No. 20123402110037), and the Chinese National 973 Fundamental Science Programs (973 program; 2015CB857004).

REFERENCES

Aihara, H., Allende Prieto, C., An, D., et al. 2011, ApJS, 193, 29
Baldry, I. K., Glazebrook, K., Brinkmann, J., et al. 2004, ApJ, 600, 681
Barazza, F. D., Binggeli, B., & Jerjen, H. 2002, A&A, 391, 823
Bertin, E., & Arnouts, S. 1996, A&AS, 117, 393
Bournaud, F., Perret, V., Renaud, F., et al. 2014, ApJ, 780, 57
Boselli, A., & Gavazzi, G. 2014, A&ARv, 22, 74
Brinchmann, J., Charlot, S., White, S. D. M., et al. 2004, MNRAS, 351, 1151
Cid Fernandes, R., Pérez, E., García Benito, R., et al. 2013, A&A, 557, 86
Croton, D. J., Springel, V., White, S. D. M., et al. 2006, MNRAS, 365, 11
Dekel, A., & Burkert, A. 2014, MNRAS, 438, 1870
Faber, S. M., Willmer, C. N. A., Wolf, C., et al. 2007, ApJ, 665, 265
Gallart, C., Stetson, P. B., Meschin, I. P., Pont, F., & Hardy, E. 2008, ApJL, 682, L89
Geach, J. E., Hickox, R. C., Diamond-Stanic, A. M., et al. 2014, Natur, 516, 68
Geha, M., Blanton, M. R., Yan, R., & Tinker, J. L. 2012, ApJ, 757, 85
Gunn, J. E., & Gott, J. R., III 1972, ApJ, 176, 1
Kauffmann, G., Heckman, T. M., Budavári, T., et al. 2007, ApJS, 173, 357
Kauffmann, G., Heckman, T. M., Tremonti, C., et al. 2003b, MNRAS, 346, 1055

Kauffmann, G., White, S. D. M., Heckman, T. M., et al. 2003a, MNRAS, 341, 54
Kaviraj, S., Rey, S.-C., Rich, R. M., Yoon, S.-J., & Yi, S. K. 2007a, MNRAS, 381, L74
Kaviraj, S., Schawinski, K., Devriendt, J. E. G., et al. 2007b, ApJS, 173, 619
Kong, X., Zhou, X., Chen, J., et al. 2000, AJ, 119, 2745
Kroupa, P. 2001, MNRAS, 322, 231
Lin, L., Zou, H., Kong, X., et al. 2013, ApJ, 769, 127
Lisker, T., Grebel, E. K., Binggeli, B., & Glatt, K. 2007, ApJ, 660, 1186
Martin, D. C., Fanson, J., Schiminovich, D., et al. 2005, ApJL, 619, L1
Mok, A., Balogh, M. L., McGee, S. L., et al. 2013, MNRAS, 431, 1090
Pan, Z., Kong, X., & Fan, L. 2013, ApJ, 776, 14
Pan, Z., Li, J., Lin, W., Wang, J., & Kong, X. 2014, ApJL, 792, L4
Pérez, E., Cid Fernandes, R., González Delgado, R. M., et al. 2013, ApJL, 764, L1
Sánchez-Blázquez, P., Forbes, D. A., Strader, J., Brodie, J., & Proctor, R. 2007, MNRAS, 377, 75
Sánchez-Blázquez, P., Rosales-Ortega, F. F., Méndez-Abreu, J., et al. 2014, A&A, 570, 6
Sánchez, S. F., Kennicutt, R. C., Gil de Paz, A., et al. 2012, A&A, 538, 8
Schawinski, K., Urry, C. M., Virani, S., et al. 2010, ApJ, 711, 284
Schawinski, K., Urry, C. M., Simmons, B. D., et al. 2014, MNRAS, 440, 889S
Schlegel, D. J., Finkbeiner, D. P., & Davis, M. 1998, ApJ, 500, 525S
Strateva, I., Ivezić, Ž., Knapp, G. R., et al. 2001, AJ, 122, 1861
Suh, H., Jeong, H., Oh, K., et al. 2010, ApJS, 187, 374
Vulcani, B., Poggianti, B. M., Fritz, J., et al. 2015, ApJ, 798, 52
Wang, J., Overzier, R., Kauffmann, G., von der Linden, A., & Kong, X. 2010, MNRAS, 401, 433
Wang, J., Kauffmann, G., Overzier, R., et al. 2011, MNRAS, 412, 1081W
Weinmann, S. M., Kauffmann, G., van den Bosch, F. C., et al. 2009, MNRAS, 394, 1213
Worthey, G. 1994, ApJS, 111, 377
Yang, Y., Zabludoff, A. I., Zaritsky, D., & Mihos, J. C. 2008, ApJ, 688, 945
York, D. G., Adelman, J., Anderson, J. E., Jr., et al. 2000, AJ, 120, 1579
Zhang, H.-X., Hunter, D. A., Elmegreen, B. G., Gao, Y., & Schruba, A. 2012, AJ, 143, 47
Zhang, W., Li, C., Kauffmann, G., & Xiao, T. 2013, MNRAS, 429, 2191